The Quinault Blowdown

A Microscale Wind Event Driven by a Mountain-Wave Rotor

Clifford F. Mass, Robert Conrick, Nicholas Weber, and Joseph P. Zagrodnik

During the early morning hours of 27 January 2018, extreme winds struck a small area on the forested slopes just north of Lake Quinault, located on the southwest side of the Olympic Mountains of Washington State (Fig. 1). In an area roughly 0.5 km^2, massive old-growth trees, some of which had stood for hundreds of years, were snapped off or uprooted. The resulting damage closed a portion of the road along the north shore of the lake and caused power outages affecting hundreds of customers. Photographs by Olympic National Park personnel and others showed numerous treefalls, documenting both the large size of some of the fallen trees and the extraordinary force required to damage them (Fig. 2).

Based on the timing of power outages and the reports of nearby residents, it appears that the strong winds were highly transient, occurring for only a few minutes around 0130 Pacific standard time (PST; 0930 UTC) 27 January 2018. A nearby seismograph of the Pacific Northwest Seismic Network (B014), located about 3 km northeast of the treefall location (Fig. 1b), observed a 4-min period of strong tremors starting around 0926 UTC 27 January 2018, with two additional impulses approximately 1 h later (Fig. 3). According to local seismologists (J. Vidale and P. Bodin, past and current directors of the Pacific Northwest Seismic Network, 2018, personal communications) the intense, sudden impulses were likely from large falling trees and the few minutes of more modest signal were the result of very strong winds interacting with the surface (Pryor et al. 2014).

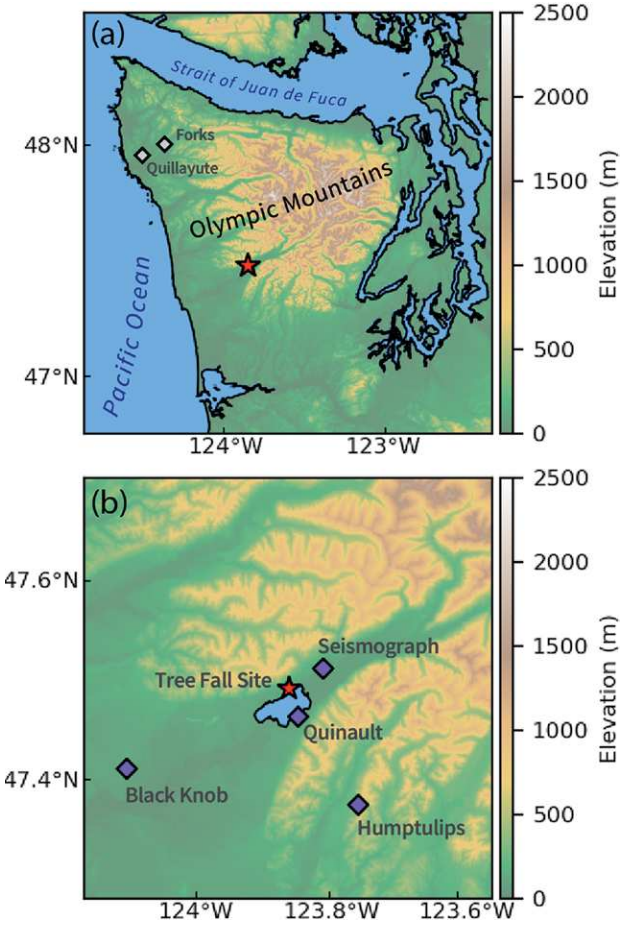

Fig. 1. (a) View of the regional geography, with a red star indicating the location of the downed trees. (b) A closer view showing Lake Quinault, the surrounding terrain, and ground sites referenced in this study. The Forks profiler and Quillayute radiosonde sites are also shown in (a).

Based on limited ground reconnaissance and a low-altitude aircraft survey, it was found that the area of damage was spatially limited, extending approximately 500 m along the north shore of Lake Quinault

AFFILIATIONS: Mass, Conrick, Weber, and Zagrodnik—Department of Atmospheric Sciences, University of Washington, Seattle, Washington
CORRESPONDING AUTHOR: Clifford F. Mass, cmass@uw.edu

DOI:10.1175/BAMS-D-18-0232.1

Fig. 2. Photographs of damaged and fallen trees taken on the north shore of Lake Quinault. [Pictures are courtesy of B. Baccus, National Park Service (top) and K. Roper (bottom).]

and a similar distance up the adjacent slope to the northwest. Fallen trees were found in 10–100-m swaths within the damage region, with most trees falling to the south-southeast, thus suggesting a wind from the north-northwest (Fig. 4). As described in the next section, strong northerly winds are unusual in this area, with the highest wind velocities generally from the south or southwest.

The initial speculation was that the small area of treefall was the result of a convectively driven microburst. However, imagery from the nearby Langley Hill radar did not support this conjecture, since generally stratiform precipitation was observed with the approaching occluded front (Fig. 5a). As described below, no low-elevation observing site in the region noted winds exceeding 20 kt (where 1 kt ≈ 0.51 m s^{-1}), leaving the origin of the powerful and damaging northerly winds unexplained. One of the most amusing aspects of

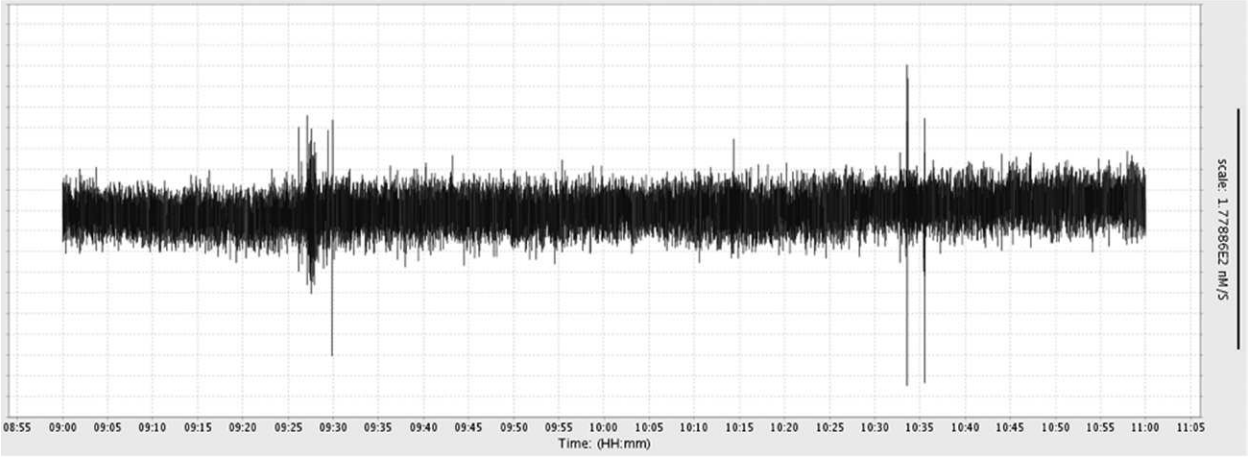

Fig. 3. Seismic signal from 0855 to 1105 UTC 27 Jan 2018 at the Pacific Northwest Seismic Network site located 3 km northeast of Lake Quinault. Location shown in Fig. 1b.

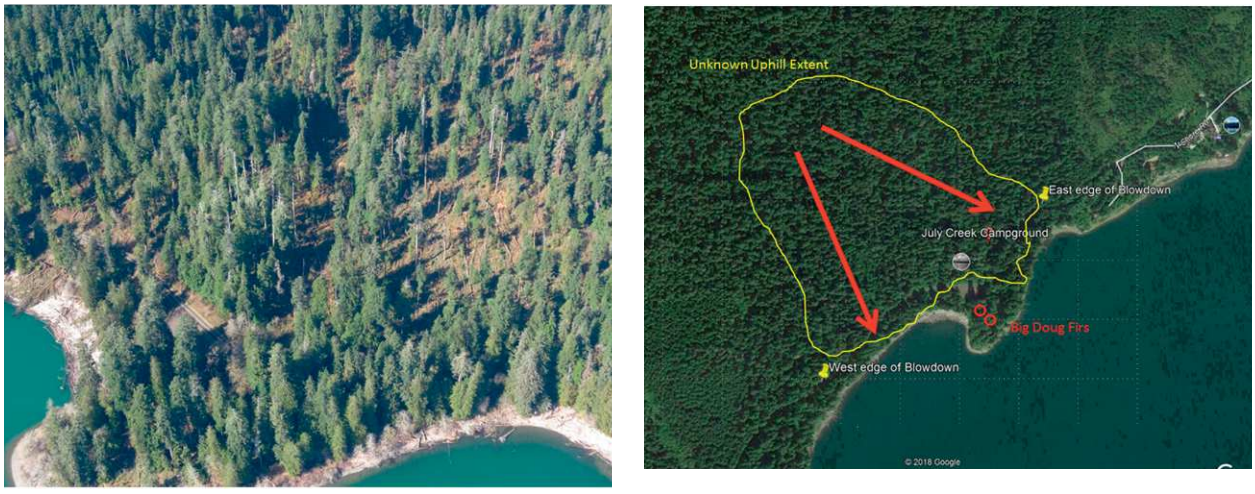

Fig. 4. (left) View of a portion of the treefall area taken from the air on 20 Mar 2018 showing swaths of tree loss. (right) Map of the approximate tree damage area based on ground surveys by National Park Service personnel, with arrows showing the direction of treefall.

the tree blowdown was the numerous suggestions in social media of unconventional origins of the event, such as U.S. military operations, aliens and unidentified flying objects, meteors, and even the actions of an angry Sasquatch.

This paper describes the synoptic and mesoscale meteorology accompanying this event and examines mechanisms that might produce a highly localized area of strong northerly winds near Lake Quinault. High-resolution model simulations are presented to elucidate the microscale processes that are inadequately captured by the sparse observations and operational models.

CLIMATOLOGICAL AND OBSERVED SURFACE WINDS. Although there are no long-term surface observing sites with wind speed and direction within or near the treefall area, two U.S. Department of Agriculture (USDA) Forest Service Remote Automated Weather Station (RAWS) locations are within 25 km. Extended-period wind roses for both locations over their period of record do not suggest a history of strong northerly winds (Fig. 6). The Black Knob RAWS site (2003–18), located on a coastal foothill of the Olympics about 20 km southeast of the damage site at an elevation of 588 ft (179 m) MSL (Fig. 1b), has both its most

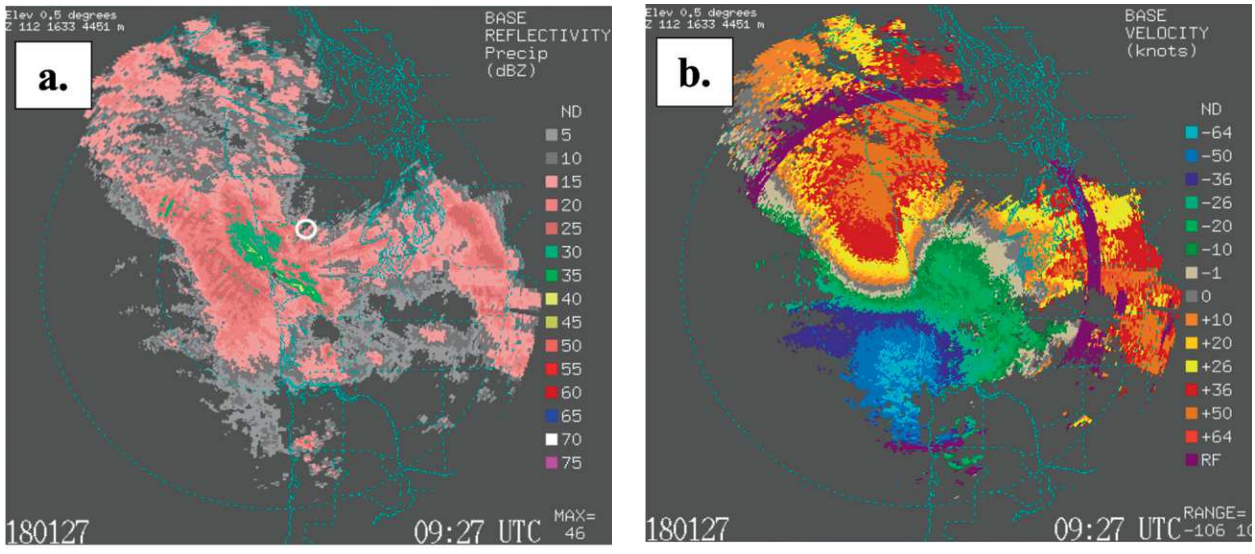

Fig. 5. (a) Radar reflectivity and (b) radial velocity at 0927 UTC 27 Jan 2018 from the 0.5° scan of the National Weather Service Langley Hill radar. The white circle shows the location of the treefalls.

frequent and strongest winds (exceeding 40 kt) from the south–southeast, with a lesser frequency peak of 20 kt from the north-northwest direction (Fig. 6a). Winds at the more exposed and higher-elevation Humptulips site [2,400 ft (750 m) ASL; 1985–2018], located on a ridge approximately 20 km southeast of Lake Quinault (Fig. 1b), are most often from the southwest, with peak wind speeds exceeding 40 kt (Fig. 6b). Northerly winds at Humptulips are infrequent and have not exceeded 20 kt during the period of record.

a. Black Knob, Washington

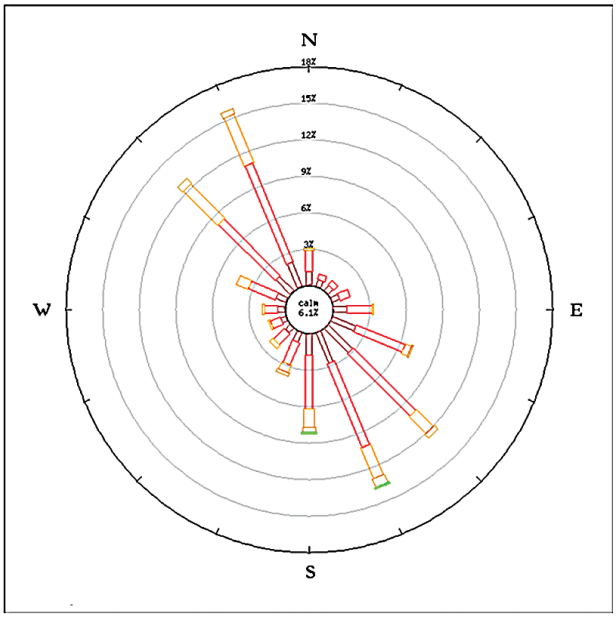

b. Humptulips, Washington

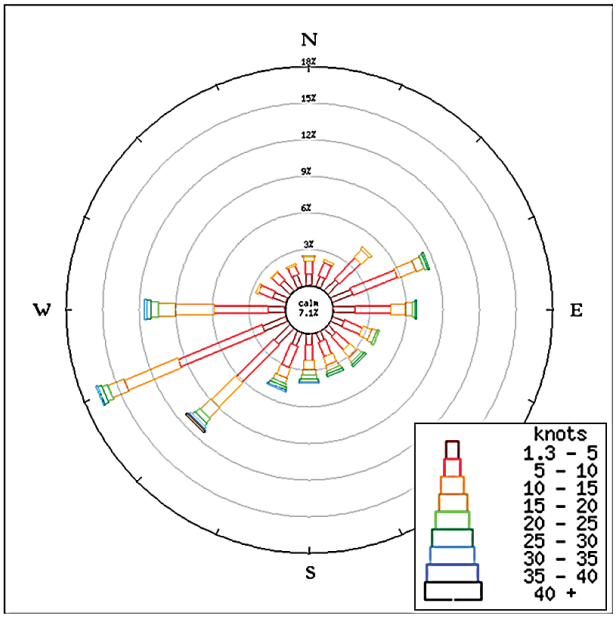

Fig. 6. Wind roses of maximum wind gusts (kt) for the period of record for the USDA/Forest Service RAWS sites at (a) Black Knob (2003–18) and (b) Humptullips (1985–2018).

There were no surface wind observation sites within the localized region of strong winds on 27 January 2018, and none of the nearby surface observing sites reported extreme winds at 0900 UTC, immediately before the blowdown. The nearest surface observing location, located in a clearing adjacent to the seismograph (Fig. 1b), is the Quinault Climate Reference Site. This station lacks wind direction but reported a maximum gust over a 10-s period at 1.5 m (not the standard 10 m) of 5.76 m s^{-1} (11.2 kt) between 0800 and 1000 UTC.

The Weather Underground station at Quinault (KWAQUINA2), located on the south side of Lake Quinault (3.5 km south of the damage location; Fig. 1b), had a peak gust of 4.37 m s^{-1} (8.5 kt) from the southwest at 0855 UTC, although the quality of this instrument is uncertain (Fig. 7). Wind direction at this location became more erratic after 0900 UTC, jumping between south-southwesterly and northeasterly during the period of strongest winds at the treefall location (~0925 UTC 27 January). Intriguingly, the sea level pressure there showed a transient, short-period dip of ~2 hPa around the time of the wind event, a possible indicator of a high-amplitude mountain wave (e.g., Sheridan et al. 2007). Farther from the damage location and toward the coast, the Black Knob RAWS site (Fig. 1b) had a maximum gust of approximately 17 kt from the southeast at the time of the incident, while the upwind, higher-elevation Humptulips RAWS site, to the southwest of the treefall, had a maximum gust of 11.3 kt from the northeast at that time. The radial velocity data from the 0.5°-elevation angle at the Langley Hill radar, located 43 km to the southwest of the treefall site, indicated a veering wind with height in the lower troposphere and a low-level (below 1 km) jet with a maximum sustained wind speed of approximately 26 kt from the southeast at the time of the treefall (Fig. 5b). There was no evidence of low-level southeasterly flow offshore, where the flow was more southerly and possessed a stronger speed maximum of approximately 50 kt at roughly 1,500 m MSL.

Determination of the localized wind speeds required to produce the substantial treefalls that morning is difficult, since tree damage depends on many factors including exposure, the directional frequency

of the climatological winds versus the direction of the wind during the event, the health of the fallen trees, and soil saturation (Mitchell 2013). In this case, the strong winds came from an unusual direction (northerly), in contrast to the southerly or southwesterly winds typically associated with the climatologically most intense winds in the area. A subjective evaluation of the photographic evidence by a local expert in wind-caused treefall (Dr. W. Read 2018, personal communication) suggested gusts of 40–50 kt or more were necessary, particularly considering the large size [8–10-ft (2.4–3.0-m) diameter] of several of the downed trees.

SYNOPTIC EVOLUTION ACCOMPANYING THE WIND EVENT. An occluded front approached the treefall location during the early morning hours of 27 January, as suggested by the tongue of warm air extending into a 999-hPa low center positioned west of the Washington coast in the 9-h forecast of the 12-km grid-spacing University of Washington (UW) Weather Research and Forecasting (WRF) Model simulation[1] initialized at 0000 UTC 27 January 2018 (Fig. 8a). A close-up view from the 1.33-km WRF domain shows a front offshore of the southern Washington coast and moderate southeasterly flow (~20 kt) at the surface approaching the treefall site (Fig. 8b).

The National Oceanic and Atmospheric Administration (NOAA) Earth System Research Laboratory (ESRL) 449-MHz radar–wind profiler observations at Forks (located 17 km east-northeast of Quillayute in Fig. 1) clearly showed the occluded frontal passage, with a veering wind and a transition to warmer temperatures (Fig. 9a). Before the frontal passage, which occurred between 0900 and 1000 UTC, there was southerly–southeasterly flow of 15–50 kt in the lowest 1.5 km of the atmosphere. No northerly wind was evident at any level. The virtual temperature near the surface at Forks warmed by 3°–4°C with the front, with greater warming aloft. The sounding data at 1200 UTC 27 January 2018 (launched at approximately 1100 UTC) from the nearby Quillayute rawinsonde (position shown in Fig. 1a) indicates a well-defined frontal inversion between 925 and 910 hPa (Fig. 9b). There was significant wind veering with height associated with the front, with strong flow (~50 kt) above the inversion and 20–50-kt winds below.

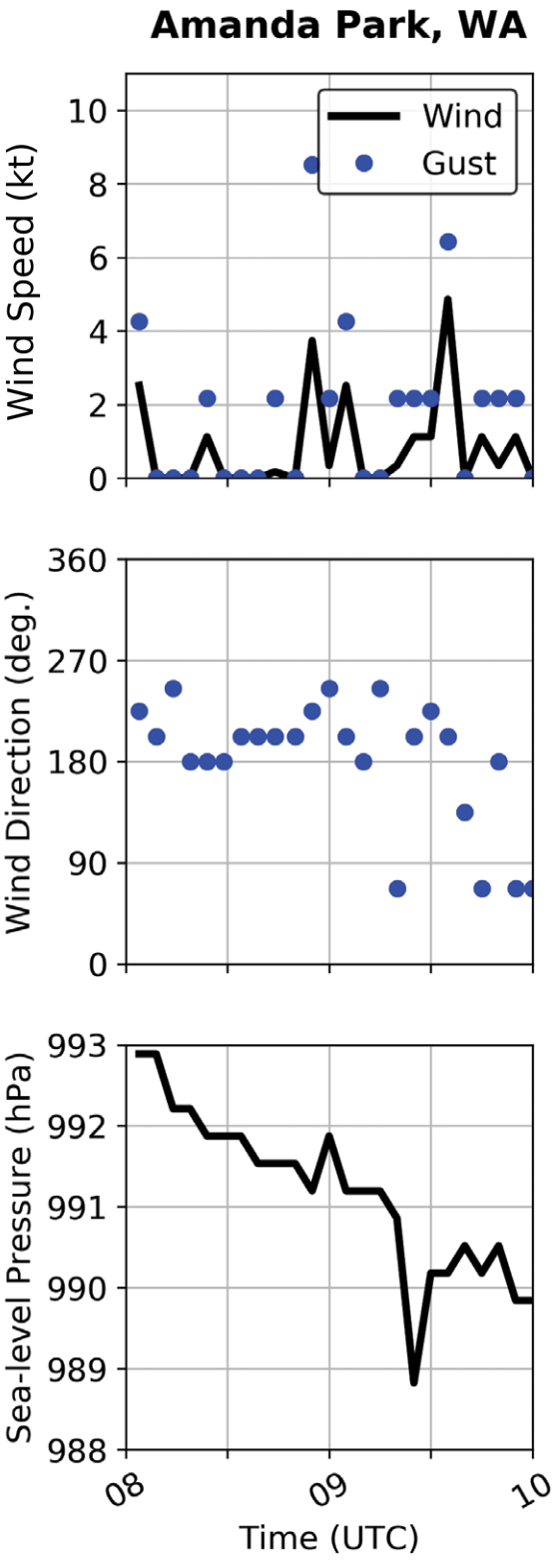

Fig. 7. Observations of wind speed (kt), wind direction, and sea level pressure (hPa) at the Quinault Weather Underground site (Fig. 1b; ID: KWAQQINA2) for 0800–1000 UTC 27 Jan 2018.

[1] For more information about the UW WRF, visit http://atmos.washington.edu/wrfrt/.

HIGH-RESOLUTION SIMULATION OF THE EVENT. To examine the origin of this high-wind event, WRF was run using 148-m horizontal grid spacing and 101 vertical levels. This simulation was initialized at 0000 UTC 27 January 2018, nested with 12-, 4-, and 1.33-km grid spacing for the outer domains, and receiving initial and boundary conditions from the National Weather Service Global Forecast System (GFS) model (0.5° grid). The terrain resolution (grid spacing) was 30 arc s, approximately 1 km. Like the operational UW WRF, this simulation used the Yonsei University (YSU) boundary/surface layer scheme (Hong et al. 2006), Thompson et al. (2008) microphysics, and the Noah land surface model with multiparameterization options (Noah-MP; Niu et al. 2011). Analysis of model output at 1-min temporal resolution revealed the development of a mountain wave and downslope flow, followed by the appearance of a rotor beginning at 0923 UTC. The rotor winds reached a maximum near the surface at 0925 UTC and the rotor dissipated by 0926 UTC, starting close to the observed initiation time

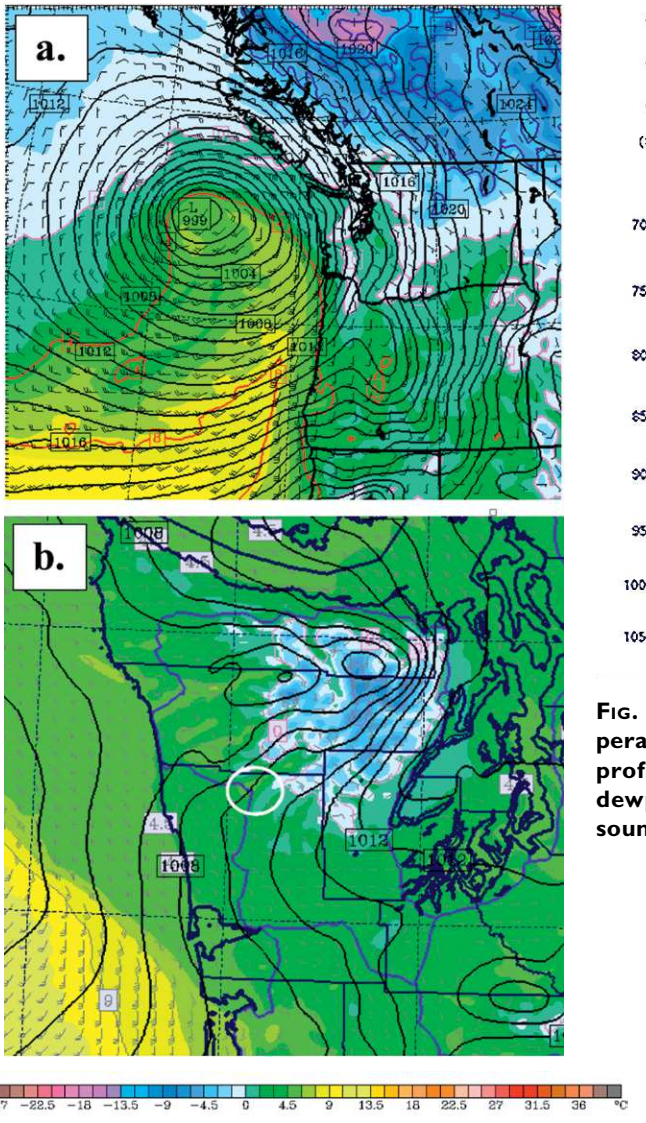

FIG. 8. The UW WRF simulations of sea level pressure (solid lines, hPa), 10-m winds (kt), and 925-hPa temperature (°C) for (a) the 9-h forecast (valid 0900 UTC 27 Jan 2018) from the 12-km domain and (b) the 10-h forecast (valid 1000 UTC 27 Jan 2018) from the 1.33-km domain. The white circle is centered on the area of tree loss.

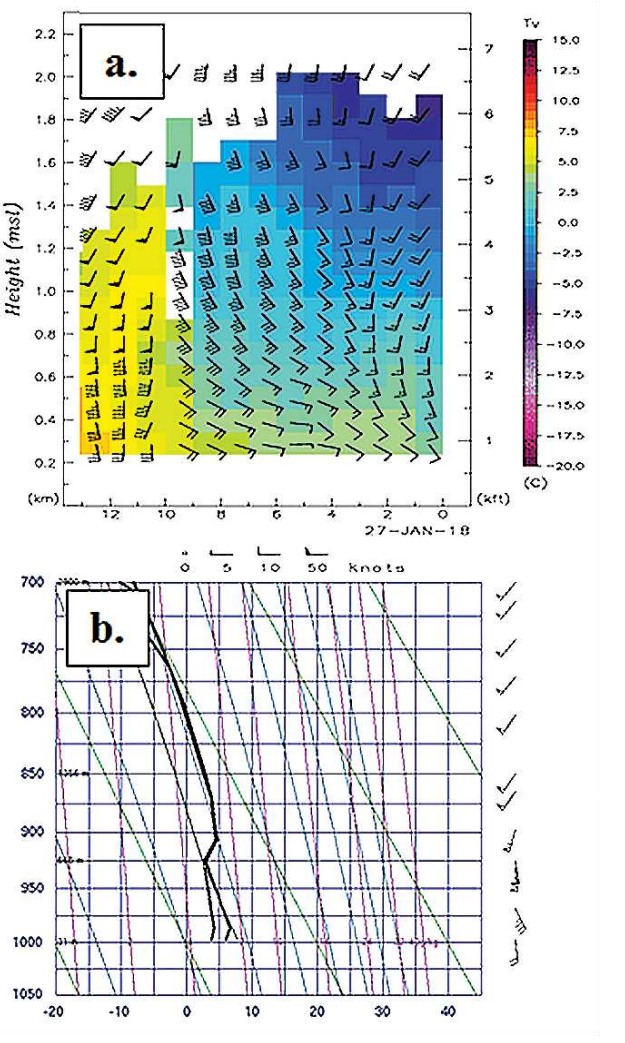

FIG. 9. (a) Wind speed and direction and virtual temperature (°C) from the NOAA/ESRL 449-MHz vertical profiler. (b) Vertical sounding of temperature (°C), dewpoint (°C), and winds (kt) from the Quillayute sounding at 1200 UTC 27 Jan 2018.

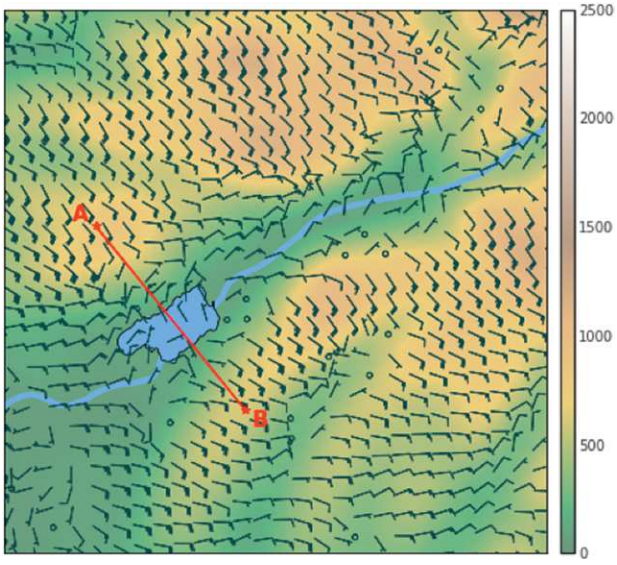

Fig. 10. The 10-m winds (kt) at 0925 UTC 27 Jan 2018 from the 148-m WRF domain, terrain elevation (m; color shading), and vertical cross-sectional location across Lake Quinault (red line).

of strong winds. Figure 10 shows simulated 10-m winds from the 148-m domain at 0925 UTC 27 January 2018, approximately the time of the observed event. Modest (~15 kt) southeasterly sustained winds were predicted over the upstream ridge, with northerly winds at and immediately north of the treefall location.

The existence of a low-level rotor is shown explicitly in a vertical cross section (location shown in Fig. 10) extending to 2,000 m MSL across the Quinault valley at the time of the wind event (0925 UTC 27 January) (Fig. 11). A terrain-induced mountain wave and near-surface rotor is evident, with 16–20 m s^{-1} winds approaching the crest of the upstream ridge. Associated with the rotor are northerly low-level winds reaching 16–18 m s^{-1} within the lowest few hundred meters over the northern side of the valley.

To explore the evolution of the synoptic and mesoscale environments that led to the wind-rotor event, Fig. 12 shows sea level pressure and 925-hPa temperatures, vertical cross sections across the Quinault valley, and upstream soundings for the 4 h prior to the event, using the output from the 1.33-km UW WRF simulation initialized at 0000 UTC 27 January 2018. The synoptic maps (left column in Fig. 12) show the approaching occluded front and the associated tongue of warm air. The corresponding vertical cross sections across the valley (middle column) exhibit a substantial increase in wind speed at and above the upstream ridge during the hours leading to the event. Finally, model vertical soundings (right column in Fig. 12) at point B, just upstream of the upwind ridge, indicate a saturated lower atmosphere and an increase in stability above the upwind ridge prior to the event (0600–0900 UTC 27 January).

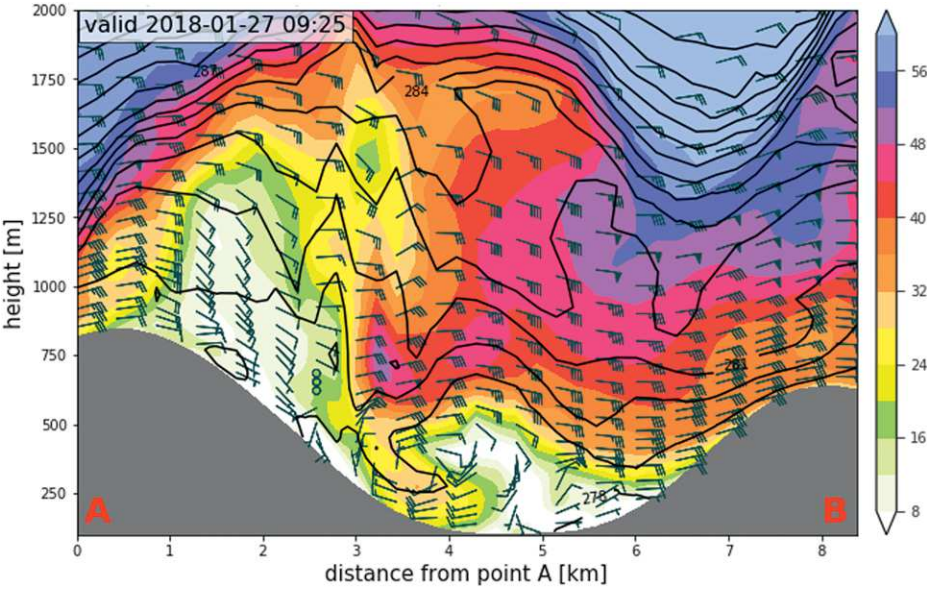

Fig. 11. Vertical cross section across the Quinault valley (line A–B in Fig. 10) at 0925 UTC 27 Jan 2018 showing the winds in the plane of the cross section (kt; barbs), potential temperature (solid lines, every 1°C), and wind speed (kt; shading).

DISCUSSION AND SUMMARY. This paper describes a highly localized strong wind event that occurred along the north shore of Lake Quinault, Washington, which is located in a valley on the southwest side of the Olympic Mountains. Strong northerly winds resulted in the loss of large trees over an area of approximately 0.5 km^2. These winds were highly transient, lasting only a few minutes starting around 0925 UTC 27 January 2018 and were not observed at surface

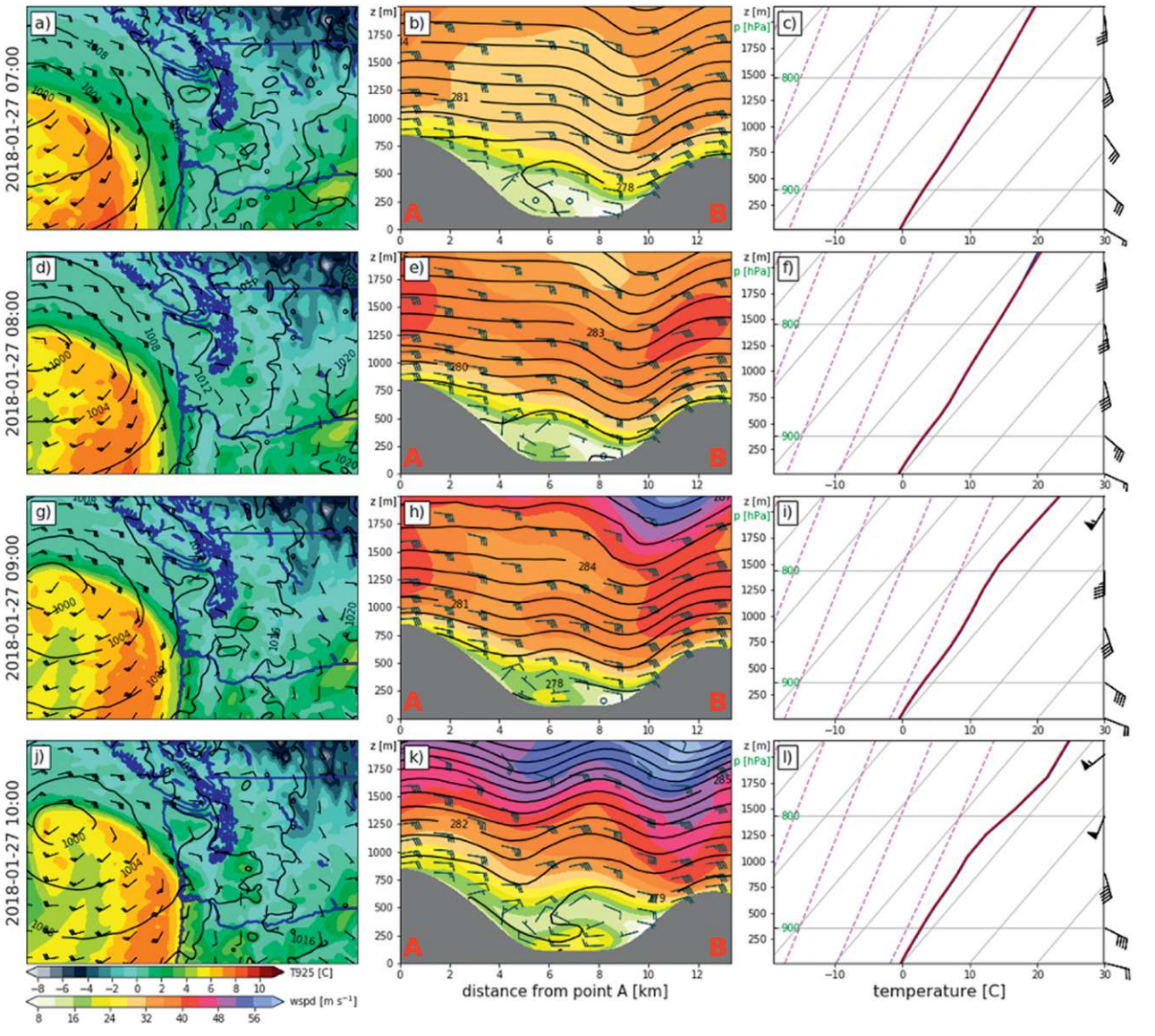

Fig. 12. (left) Sea level pressure (hPa), 925-hPa temperature (°C), and 10-m winds (kt). (middle) Vertical cross section across the Quinault valley (location shown in Fig. 10) for total wind speed (kt; color shading), wind along the cross section (kt; wind barbs), and potential temperature (K). (right) Upstream model soundings at point B showing temperature and dewpoint (°C; red and blue lines) and horizontal winds (kt). The sounding is at water saturation throughout the layer shown above. Results at 0700, 0800, 0900, and 1000 UTC 27 Jan are shown.

stations in the surrounding area. This event was associated with the approach of a Pacific occluded front that produced moderate (15–30 kt) low-level southeasterly flow and a stable layer with wind veering with height above the crest of the upwind terrain (Fig. 9b). This upstream environment is favorable for high-amplitude wave and rotor formation (e.g., Doyle and Durran 2002; Grubišić and Billings 2007).

An important feature of the event was the strong northerly winds during the period of treefall, in contrast to the general southerly–southeasterly mesoscale/synoptic winds of the region. Strong northerly winds are unusual in the area of treefall, and it is expected that the trees were more vulnerable to damage from an unaccustomed direction. Regional pressure gradients were modest (Fig. 8b) and consistent with southeasterly winds and, thus, cannot explain the strong northerly flow. High-resolution WRF simulations produced moderate northerly flow in the correct location (north of Lake Quinault) and time as the

event, resulting from a high-amplitude mountain wave and attendant rotor within the valley. The rotor was produced by the interaction of incoming southeasterly flow with a southwest–northeast-oriented ridge to the southeast of the damage site (Fig. 1).

While the timing and location of the northerly rotor-driven wind event were well captured by the 148-m WRF simulation, the maximum near-surface model wind speed [16–18 m s^{-1} (31–35 kt)] was too low. It appears that 148-m grid spacing is not sufficient for properly defining the intensity and tight structure of the rotor circulation and is within a resolution gray zone for which the assumptions made in contemporary boundary layer parameterizations are probably not valid. It might well be expected that a large-eddy simulation (LES), using resolutions in which turbulent eddies are resolved (10–20-m grid spacing), might not only better simulate the major rotor circulation, but also define subrotors that produce much stronger transient winds (Doyle and Durran 2002, 2007; Doyle et al. 2009; Cohn et al. 2011; Strauss et al. 2016). The nearly perfect timing of such a complex mesoscale flow event was fortuitous, although a timing error of less than an hour might be expected considering the strong control of the synoptic-scale forcing from the approaching front.

An important question concerns the frequency of this localized treefall event and whether the synoptic/mesoscale conditions during the event were unusual. Such localized, low-elevation tree loss with northerly winds has not been noted previously in the immediate area (B. Baccus, National Park Service, 2018, personal communication) and the frequency of intense, transient, microscale rotors in nearby mountain valleys is uncertain. Since mountain-wave amplification is often related to elevated stable layers near and above crest level and strong winds approaching terrain (Doyle and Durran 2002), we compared the 27 January 2018 event with other dates that had lower-tropospheric inversions. Specifically, we considered several parameters (925–850-hPa wind shear, inversion bottom height, maximum wind speed below the inversion) and used observations from the nearby soundings at Quillayute, Washington (Fig. 1a).

Figure 13 shows a plot of three of these parameters at Quillayute based on observations between 1995 and 2018 for the months of October–March, with the star indicating the observation at 1200 UTC 27 January. Only days with a nonsurface inversion of at least 1°C were considered, resulting

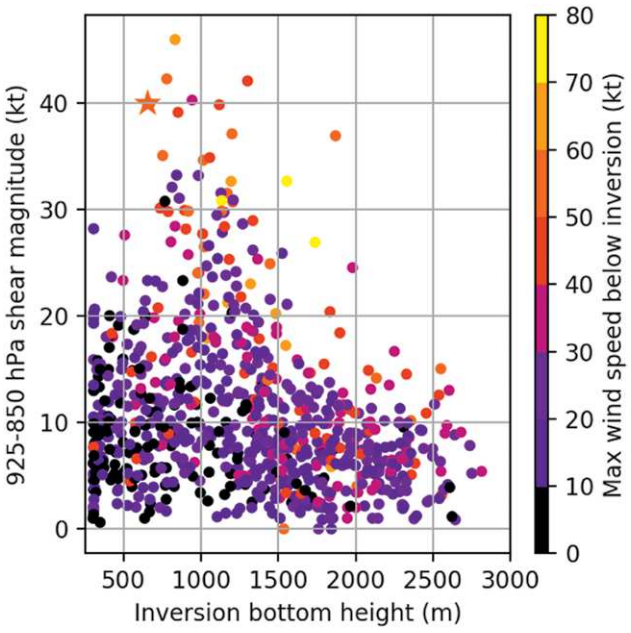

Fig. 13. Scatter diagram of the height of the inversion bottom (m) and 925–850-hPa wind shear magnitude (kt) based on Quillayute soundings (Fig. 1a) for periods with low-level inversions during 1995–2018. The points are color coded to show the maximum wind speed below the inversion (kt). The star indicates 1200 UTC 27 Jan 2018.

in 800 soundings. It is clear from Fig. 13 that conditions on the morning of 27 January 2018 were unusual. The 925–850-hPa wind speed shear (40 kt) was near the highest on record at that location (925 hPa is close to the height of the upwind terrain), and the height of the inversion base was relatively low and nearly identical to the height of the upstream terrain. In short, the combination of strong wind shear and a low inversion base, with the latter nearly coincident with the height of the upstream terrain, is highly unusual and favorable for the formation of downstream vorticity that can be expressed in rotor circulations and localized strong winds.

Future work on this event should include LES simulations to determine whether considerably higher wind speeds might result from better defining the rotor and possible subrotors, and the exploration of the sensitivity of rotor location and amplitude to variations in the incoming flow. In any case, the ability of a simulation with marginal resolution (148-m grid spacing) to capture the occurrence of a rotor at almost exactly the correct time and location is a favorable sign for the potential to predict future

occurrences of such infrequent, but potentially destructive, localized phenomena.

ACKNOWLEDGMENTS. We received substantial advice and assistance from Mr. Bill Baccus and Ms. Janet Coles of Olympic National Park, who made us aware of the event and its effects on vegetation; Dr. Wolf Read regarding the details of wind-related treefall; and Professor Dale Durran on rotor generation. Mr. Tom Jensen graciously flew us in his own aircraft for an aerial survey of the site. We acknowledge support from NSF Grant AGS-1349847.

FOR FURTHER READING

Cohn, S. A., V. Grubišić, and W. O. J. Brown, 2011: Wind profiler observations of mountain waves and rotors during T-REX. *J. Appl. Meteor. Climatol.,* **50,** 826–843, https://doi.org/10.1175/2010JAMC2611.1.

Doyle, J. D., and D. R. Durran, 2002: The dynamics of mountain-wave-induced rotors. *J. Atmos. Sci.,* **59,** 186–201, https://doi.org/10.1175/1520-0469(2002)059<0186:TDOMWI>2.0.CO;2.

——, and ——, 2007: Rotor and subrotor dynamics in the lee of three-dimensional terrain. *J. Atmos. Sci.,* **64,** 4202–4221, https://doi.org/10.1175/2007JAS2352.1.

——, V. Grubišić, W. O. Brown, S. F. De Wekker, A. Dörnbrack, Q. Jiang, S. D. Mayor, and M. Weissmann, 2009: Observations and numerical simulations of subrotor vortices during T-REX. *J. Atmos. Sci.,* **66,** 1229–1249, https://doi.org/10.1175/2008JAS2933.1.

Grubišić, V., and B. J. Billings, 2007: The intense lee-wave rotor event of Sierra Rotors IOP 8. *J. Atmos. Sci.,* **64,** 4178–4201, https://doi.org/10.1175/2006JAS2008.1.

Hong, S.-Y., Y. Noh, and J. Dudhia, 2006: A new vertical diffusion package with an explicit treatment of entrainment processes. *Mon. Wea. Rev.,* **134,** 2318–2341, https://doi.org/10.1175/MWR3199.1.

Kühnlein, C., A. Dörnbrack, and M. Weissmann, 2013: High-resolution Doppler lidar observations of transient downslope flows and rotors. *Mon. Wea. Rev.,* **141,** 3257–3272, https://doi.org/10.1175/MWR-D-12-00260.1.

Mitchell, S. J., 2013: Wind as a natural disturbance agent in forests: A synthesis. *Forestry,* **86,** 147–157, https://doi.org/10.1093/forestry/cps058.

Niu, G.-Y., and Coauthors, 2011: The community Noah land surface model with multiparameterization options (Noah-MP): 1. Model description and evaluation with local-scale measurements. *J. Geophys. Res.,* **116,** https://doi.org/10.1029/2010JD015139.

Pryor, S. C., R. Conrick, C. Miller, J. Tytell, and R. J. Barthelmie, 2014: Intense and extreme wind speeds observed by anemometer and seismic networks: An eastern U.S. case study. *J. Appl. Meteor. Climatol.,* **53,** 2417–2429, https://doi.org/10.1175/JAMC-D-14-0091.1.

Sheridan, P. F., V. Horlacher, G. G. Rooney, P. Hignett, S. D. Mobbs, and S. B. Vosper, 2007: Influence of lee waves on the near-surface flow downwind of the Pennines. *Quart. J. Roy. Meteor. Soc.,* **133,** 1353–1369, https://doi.org/10.1002/qj.110.

Strauss, L., S. Serafin, and V. Grubišić, 2016: Atmospheric rotors and severe turbulence in a long deep valley. *J. Atmos. Sci.,* **73,** 1481–1506, https://doi.org/10.1175/JAS-D-15-0192.1.

Thompson, G., P. R. Field, R. M. Rasmussen, and W. D. Hall, 2008: Explicit forecasts of winter precipitation using an improved bulk microphysics scheme. Part II: Implementation of a new snow parameterization. *Mon. Wea. Rev.,* **136,** 5095–5115, https://doi.org/10.1175/2008MWR2387.1.